



**HAL**  
open science

# What happens when a Pb–Sn coating deposited on low carbon steel is exposed in an HCl-polluted wet environment? Development of a corrosion mechanism

Florence Lequien, Gervaise Moine, Arnaud Lequien, Delphine D. Neff

## ► To cite this version:

Florence Lequien, Gervaise Moine, Arnaud Lequien, Delphine D. Neff. What happens when a Pb–Sn coating deposited on low carbon steel is exposed in an HCl-polluted wet environment? Development of a corrosion mechanism. *Materials and Corrosion / Werkstoffe und Korrosion*, 2022, 73 (9), pp.1459-1473. 10.1002/maco.202213142 . cea-03681016

**HAL Id: cea-03681016**

**<https://cea.hal.science/cea-03681016>**

Submitted on 30 May 2022

**HAL** is a multi-disciplinary open access archive for the deposit and dissemination of scientific research documents, whether they are published or not. The documents may come from teaching and research institutions in France or abroad, or from public or private research centers.

L'archive ouverte pluridisciplinaire **HAL**, est destinée au dépôt et à la diffusion de documents scientifiques de niveau recherche, publiés ou non, émanant des établissements d'enseignement et de recherche français ou étrangers, des laboratoires publics ou privés.

# What happens when a Pb–Sn coating deposited on low carbon steel is exposed in an HCl-polluted wet environment? Development of a corrosion mechanism

Florence Lequien<sup>1</sup>  | Gervaise Moine<sup>1</sup> | Arnaud Lequien<sup>2</sup> | Delphine Neff<sup>3</sup>

<sup>1</sup>CEA, Service de la Corrosion et du Comportement des Matériaux dans leur Environnement, Université Paris-Saclay, Gif-sur-Yvette, France

<sup>2</sup>CEA, Service de Recherches Métallurgiques Appliquées, Université Paris-Saclay, Gif-sur-Yvette, France

<sup>3</sup>LAPA NIMBE UMR3685 LMC—IRAMAT UMR 5060, CEA/CNRS, Université Paris Saclay, Gif sur Yvette cedex, France

## Correspondence

Florence Lequien, CEA, Service de la Corrosion et du Comportement des Matériaux dans leur Environnement, 91191, Gif-sur-Yvette, France.  
Email: [florence.lequien@cea.fr](mailto:florence.lequien@cea.fr)

## Abstract

This article synthesizes all the results obtained to establish a global corrosion mechanism when a Pb–Sn coating deposited on low carbon steel is corroded in an HCl-polluted wet environment. The successive stages of the process are shown. In HCl-polluted environment, coupled with water, acid chlorides provide an aggressive electrolyte particularly favorable to corrosion. In contact with this electrolyte, lead products are created as  $\text{PbCO}_3$  and  $\text{PbCl}_2$ , showing the impact of the surrounding atmosphere. In parallel, the electrolyte concentrates in  $\text{Sn}^{2+}$  until saturation, and tin precipitates under different forms. Due to the lead consumption, the lead corrosion products layer breaks, and the coating thins, diffusion pathways are created and the steel oxidizes. Iron corrosion products are similar with or without a coating except for the presence of a tin-rich filament. Lead is no longer present. The different stages of the mechanism are compared to corrosion phenomena observed during the use of Pb–Sn alloys to provide effective solutions to minimize or even avoid the phenomenon of corrosion.

## KEYWORDS

corrosion, HCL, mechanism, Pb–Sn coating

## 1 | INTRODUCTION

The Pb–Sn alloy has been conventionally utilized as a solder material: the eutectic tin-lead alloy is used as an inter-connection alloy.<sup>[1]</sup> Historically, Pb has been mixed with tin into electronic solder materials to improve manufacturing processing and reduce the growth of Sn whiskers.<sup>[2]</sup> The alloy has received only limited attention because of the concerns of lead toxicity: elimination of lead (Pb) from electronic devices is now established as a requirement for electronic component manufacturers.<sup>[3,4]</sup> Nevertheless, recent research using the Pb–Sn alloy has demonstrated

the recycling of valuable Pb and Sn elements from electronic waste.<sup>[5–7]</sup> More generally, the Pb–Sn alloys are used in a lot of domains: Pb–Sb alloy is used as grid materials in lead-acid batteries<sup>[8]</sup> because of its good casting and deep cycling properties,<sup>[9]</sup> as shielding materials for highly penetrating radiations of gamma rays during the reactions occurring in nuclear reactors<sup>[10]</sup> or as a lubricating coating.<sup>[11]</sup>

As it is used in many domains, the Pb–Sn alloy can be exposed to different environments, potentially corrosive. In this study, we focus on a humid and HCl-polluted environment, which is a common environment in electronic,<sup>[12,13]</sup> in the manufacture of PVC<sup>[14]</sup> or many

This is an open access article under the terms of the Creative Commons Attribution-NonCommercial-NoDerivs License, which permits use and distribution in any medium, provided the original work is properly cited, the use is non-commercial and no modifications or adaptations are made.

© 2022 The Authors. *Materials and Corrosion* published by Wiley-VCH GmbH.

other fields including metal and mineral processing,<sup>[15]</sup> or waste treatments.<sup>[16,17]</sup> Chlorides in the form of hydrogen chloride facilitate the formation of thin droplets of hydrochloric acid due to the air acid condensed moisture.<sup>[18]</sup> In contact with this electrolyte, corrosion initiates.

There are only a few data points on the corrosion phenomena in an HCl-polluted environment for Pb–Sn alloys. A potentiodynamic polarization analysis carried out in a 1 M HCl solution shows the formation of tin oxide SnO, SnCl<sub>2</sub>, and lead oxide PbO<sub>2</sub> at the surface of an Sn–37Pb alloy.<sup>[19]</sup> In a solution of 2 mol/l HCl, an Sn–Pb eutectic alloy exhibits a rapid increase of the corrosion rate in the first 10 min followed by a continuous decrease.<sup>[20]</sup> For this short experiment, the stability of this alloy after the first 10 min seems to be due to the formation of mixed oxides of the lead and tin protective layer. It may prevent the continuous attack of corrosive ions. In an acidic medium, the main reaction is the ionization of lead with Pb<sup>2+</sup> formation, both for lead and Pb–Sn alloys (with an Sn content between 3.5 and 80 wt %).<sup>[21]</sup> More generally, in the HCl medium, the lead addition disfavors the corrosion resistance in comparison to pure tin, resulting in a fragile oxide layer and pitting.<sup>[22]</sup> Pits are generally related to the pH value between three and seven. Moreover, each element Pb or Sn considered separately has a poorly resistance in hydrochloric acid solution.<sup>[23]</sup>

Exposed to an environment containing gaseous contaminants, the oxidation of tin leads to the formation of tin oxides, whereas the lead presence causes the formation of corrosion products such as PbCO<sub>3</sub> or Pb(OH)<sub>2</sub>,<sup>[21]</sup> poorly protective.<sup>[24]</sup> Only 2% tin in the Pb–Sn alloy is sufficient to improve the corrosion resistance of lead. On the other hand, in moist ambient air, the 94Sn–6Pb solder reacts rapidly and forms different corrosion products like the stannous oxide (SnO) or the stannic oxide (SnO<sub>2</sub>),<sup>[25]</sup> depending on the partial oxygen pressure. The lead species are evenly distributed as lead and lead oxides. The differences in oxidation behavior following oxygen partial pressure can be explained by kinetic considerations.<sup>[26]</sup> Coupled with water from the air, the HCl(g) adsorbs in the liquid providing an aggressive electrolyte that leads to corrosion with the formation of a stressed and brittle PbCl<sub>2</sub> layer and tin precipitates in rich oxygen and chlorine plates form.<sup>[27]</sup> In parallel, tin precipitates in the form of hydrated corrosion products composed of tin, oxygen, and chlorine, such as abhurite or hydrated tin chloride, SnCl<sub>2</sub>·2H<sub>2</sub>O.<sup>[28]</sup> Nevertheless, although a few stages of the mechanism have been identified, no comprehensive mechanism that can explain the failures has been established, due to the fact that these failures are not easily detected during subsequent failure analysis.<sup>[12]</sup>

The purpose of this article is to synthesize all the results obtained to establish a global corrosion mechanism when a Pb–Sn coating deposited on low carbon steel is corroded in an HCl-polluted wet environment. The successive stages of the process will be shown, as the consequences of this corrosion phenomenon and how to minimize its impact.

## 2 | MATERIAL AND METHODS

### 2.1 | Materials

Two materials are used in the study: low carbon steel and a 75Sn–25Pb coating on low carbon steel. The idea is to focus on the 75Sn–25Pb corrosion mechanism. Comparing the bare and the coated low carbon steels shows the limits of use of such coating and its shortcomings.

For the low carbon steel, A37 steel is used and its composition is presented in Table 1. A steel sheet, 0.8 mm thickness, type FeP01 or FeP04 is used. The coating is Sn 75 wt% content with a content of Pb, which is above the eutectic composition Pb–61.9%Sn. The surface structure is made of large, well-defined white studs (Figure 1a). These are lead islands surrounded by tin, darker on scanning electron microscope (SEM) due to chemical contrast, particularly visible in the section (Figure 1b). The layer measures slightly less than 5 μm.

### 2.2 | Methods

The first three experiments are gravimetric tests in different environments.

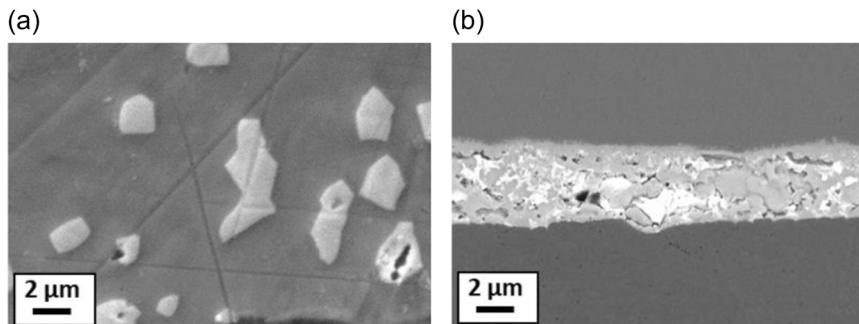
To study how materials corrode when they are only in contact with a humid air-controlled atmosphere, samples are placed in airtight container boxes in a climatic chamber maintained at 20°C. Different kinds of salt are introduced to control the relative humidity (RH): the CH<sub>3</sub>COOK salt leads to a 24% RH, K<sub>2</sub>CO<sub>3</sub> salt to 45% RH, and NaCl salt to 75% RH. Three samples of each steel are introduced per box.

To study the corrosion in solution and over, that is, in vapor/condensate phase, samples are immersed in 1 mol/l hydrochloric acid solution or placed over the solution. This concentration is chosen because 1 mol/l is in the mixed domain of weak corrosion and penalizing corrosion of the

TABLE 1 Composition of steels (wt%)

Steel	Fe	C	Mn	P	S
A37	Base	0.12	0.62	Max 0.012	Max 0.012
FeP01 or FeP04	Base	Max 0.12	Max 0.6	Max 0.045	Max 0.045

**FIGURE 1** SEM images of the 75Sn–25Pb coating on low carbon steel sample before testing: (a) top view and (b) section. SEM, scanning electron microscope.



316 L steel (a reference material).<sup>[29]</sup> By controlling the concentration and the temperature of the hydrochloric acid solution, the HCl vapor phase content is thermodynamically imposed. Experimental data provide the vapor pressures of HCl above a hydrochloric acid solution of known concentration and temperature.<sup>[18]</sup> From these data, the liquid phase/vapor phase equivalents used for the test present an HCl partial pressure over a 1 mol/l HCl of 0.19 ppm. Over a 1 mol/l HCl solution, a long test (named LT) of 1100 h was done first on both the carbon steel and the tinned steel. During this test, the samples are not observed until the test end. In parallel, to study more particularly the tinned steel corrosion initiation, other tests were done: a short test (ST) of less than 400 h (presented in detail in a precedent article) where the reactor is opened regularly and an intermediate test (IT) where the reactor is opened only after 500 h. During these tests, samples are taken out of the reactor to be analyzed at each opening. All the tests are carried out in double-shell glass reactors, with a useful volume of 2 L. The temperature is controlled by a thermostatically controlled fluid device. Many samples per environment are introduced per reactor. They are suspended on a glass support.

In these three experiments, the samples are square samples of dimensions  $20 \times 20 \times 1$  mm.

The impact of a humid air flow polluted by HCl is also studied. An original device was built.<sup>[27]</sup> The gaseous mixture is carried out in a reactor connected to two gas feedthroughs: a flow of polluted air with HCl(g) created by a pervaporation furnace and a flow of humid air from a WETSYS. The temperature is controlled using a coil, fixed at the top to avoid condensation on the walls and the lid. The lower part is thermostatically controlled, allowing located condensation. In our tests, the upper part is maintained at 23°C, and the lower at 14°C, which gives a temperature of 18°C on the samples. At the exhaust, the gas is analyzed by a ProCEas detector, which allows the monitoring of water and HCl contents in the reactor during the tests. The diameter of the specimens is 78 mm; the same for the reactor. Before testing, the sample is cleaned with ethanol in an ultrasonic bath for 15 min. It is then degreased overnight in S15 solvent

(limonene) and dried under compressed air. 3 ppm of HCl are injected continuously with a flow rate of  $200 \text{ ml min}^{-1}$ . The relative humidity was 33% RH. The humid air is injected with a flow rate of  $149 \text{ ml min}^{-1}$ .

At the test end, the corrosion phenomenon is characterized. An optical microscope is used for macroscopic observations; while microscopic investigations are carried out using a SEM equipped with an electron-dispersive spectrometry X-ray microanalysis system (EDS) for the elemental analysis of the selected areas. These analyses were supplemented by analyses done by X-ray diffraction and Raman not shown in this article.

### 3 | RESULTS

#### 3.1 | Test in a humid environment

The samples' mass variation exposed to different moist airs between 24% and 75% are presented in Figure 2 for the low carbon steel and in Figure 3 for the coated steel. Given the scale, the variations in mass are small (around  $10^{-6} \text{ g/cm}^2$ ) and close to the precision limit of the balance.

For the low carbon steel, the mass variation is positive. The mass gain is due to the local presence of corrosion products, rich in iron and oxygen.

For the 75Sn–25Pb coating, a slight change in mass appears; a mass gain at high humidity and mass loss at low or moderate humidity over the first 500 h. No change is observed thereafter. For samples exposed to the higher RH, corrosion product islands are visible locally. These are lead-rich corrosion products. The elemental composition corresponds to cerussite  $\text{PbCO}_3$  (Figure 4b). A tin native oxide  $\text{SnO}$  accompanies it. A percentage of iron, that can reach 11 wt%, is detected around the cluster of cerussite (Figure 4b). This illustrates the layer thickness variations, which locally is finer and leads to detecting a significant weight of iron. Although the percentage of oxygen is higher after testing, the overall results conclude that there is negligible corrosion of these materials in a humid environment.

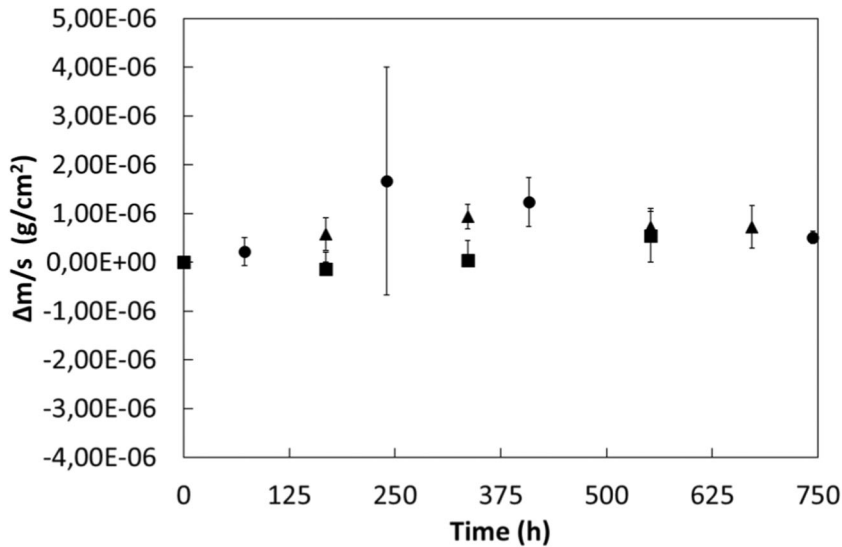


**FIGURE 2** Evolution of the mass during exposure test in moist air of the low carbon steel samples, (■) for a relative humidity of 24%, (▲) for a relative humidity of 45%, and (●) for a relative humidity of 75%.

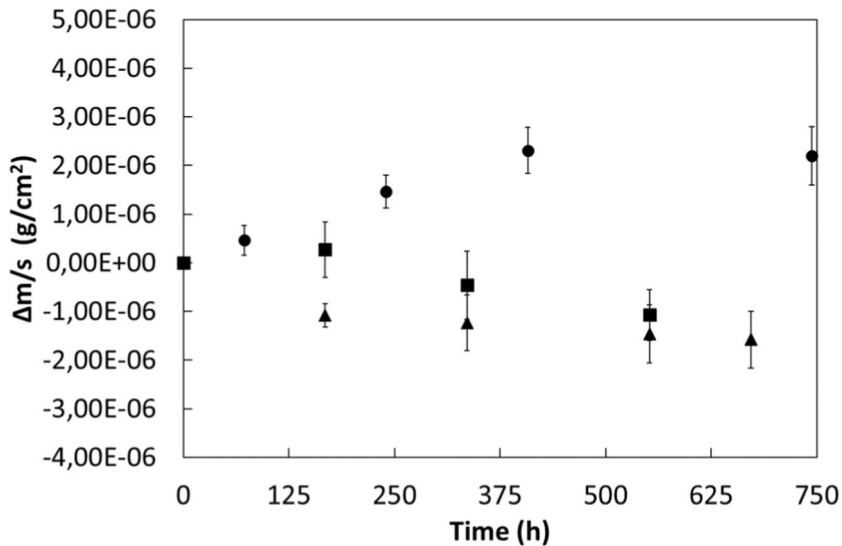


**FIGURE 3** Evolution of the mass during exposure test in moist air of the 75Sn-25Pb coating on a low carbon steel sample, (■) for a relative humidity of 24%, (▲) for a relative humidity of 45%, and (●) for a relative humidity of 75%.

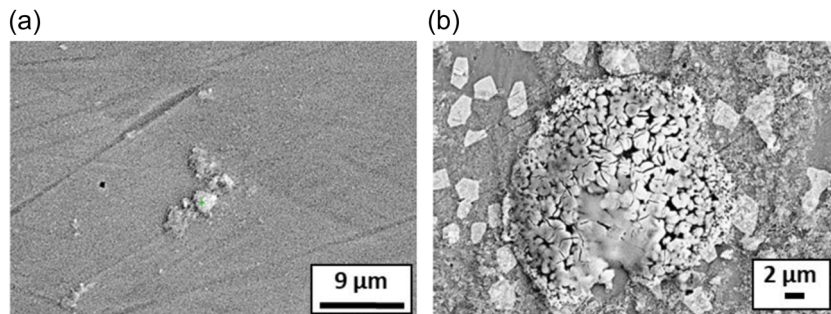
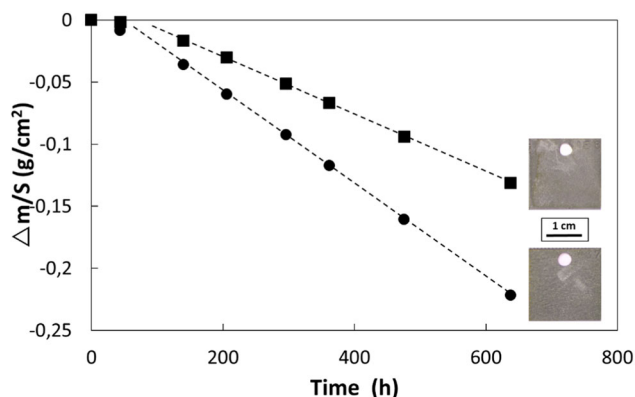


**FIGURE 4** SEM study at the test end. (a) For the low carbon steel in 45% RH and (b) for the tinned steel in 75% RH. RH, relative humidity; SEM, scanning electron microscope.

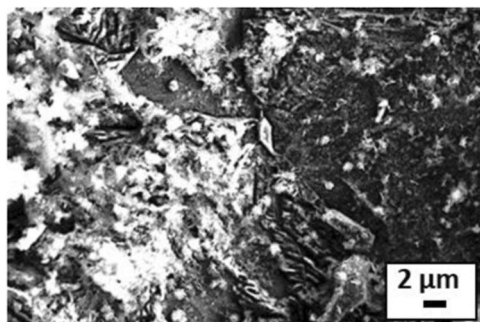
### 3.2 | Test in an HCl solution

Figure 5 presents the mass variation in 1 mol/l HCl solution. After a latency phase where the gravimetric variations are very small, the samples lose mass. This corresponds to a material dissolution. The mass losses follow a linear evolution, with a corrosion rate of

2250  $\mu\text{m}/\text{year}$  for the tinned steel and 3370  $\mu\text{m}/\text{year}$  for the low carbon steel. Even if the corrosion rate is different between the two materials, the samples' facies after testing is quite similar, as shown by the offsets in Figure 5. The entire tinning layer is dissolved. No lead or tin traces are detected on the surface (Figure 6). The coating dissolution is confirmed by the solution analysis



**FIGURE 5** Evolution of the mass during exposure test in 1 mol/l HCl solution of the 75Sn–25Pb coating on a low carbon steel specimen, coated and uncoated. The dashed line shows the linear trend of the second part of the test. (●) for the carbon steel and (■) for the tinned steel. The offset shows a macrograph of one specimen after testing.



**FIGURE 6** SEM study of the tinned steel specimen immersed 638 h in 1 mol/l HCl solution. SEM, scanning electron microscope.

**TABLE 2** Analysis of the 1 mol/L immersion solution carried out by atomic emission spectroscopy after 638 h of testing

Concentrations (g/l)	Fe	Sn	Pb
Low carbon steel	8.10		
75Sn–25Pb coating on low carbon steel	4.56	4.37 10 <sup>-02</sup>	2.12 10 <sup>-02</sup>

after testing detecting the presence of lead and tin. Tin is more concentrated than lead in accordance with the composition of the tinning layer (Table 2).

### 3.3 | Static tests in a highly humid air polluted by HCl

The mass evolution of the samples exposed in vapor/condensate phase, over a 1 mol/l HCl solution, is positive (Figure 7). It means that exposure to an HCl solution

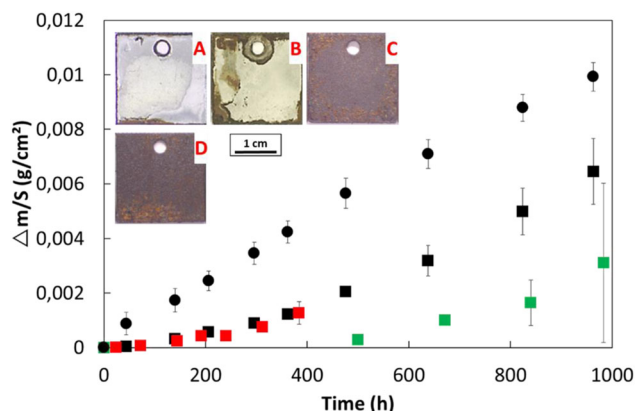


**FIGURE 7** Evolution of the mass during exposure test in vapor/condensate phase over a 1 mol/l HCl solution: (●) for the low carbon steel and (■) for the tinned steel: (red) short test, (green) for intermediate test and (black) for a long test. The offset shows a macrograph of one specimen after testing (A) for the short test, (B) for the intermediate test, (C) for the long test with the tinned steel samples, and (D) for the long test with the carbon steel samples. [Color figure can be viewed at [wileyonlinelibrary.com](http://wileyonlinelibrary.com)].

leads to corrosion product precipitation. The shortest test and the long test overlap, while the mass gain during the intermediate test is weaker. The difference is about 0.002 g/cm<sup>2</sup> over time. Nevertheless, the evolution tendency is similar. Unlike the ST and LT, during the first 500 h of the IT, the reactor is not opened, which results in a very low mass gain on the first opening after 500 h exposure.

The offset shows the samples after testing. Rust-colored oxide is present on the entire surface of steel exposing more than 1000 h. Corrosion is more marked on the bottom of the sample. In this area, the condensates gather during the test, and then fall by gravity, tearing off the oxide, poorly adherent and cracked. The SEM-EDS analysis, done on the cross-section observed in Figures 8 and 9, shows that the tinned layer is absent. The layer consists of an iron oxide base with an O-Fe ratio of 36–63 wt%. The thickness of this sublayer varies from a few microns to more than 20 μm. Locally a chloride content is detected with a maximum value of 5 wt%. As one moves away from the metal/oxide interface, the oxide structure evolves passing through a poorly crystallized phase containing ferrihydrite, to then be magnetite Fe<sub>3</sub>O<sub>4</sub>.

The difference between the low carbon steel and the tinned steel appears in the middle of the oxide layer. For the tinned steel, a white line is visible. It is a white strip of tin. In this area, a content of 60–70 wt% of tin can be measured by EDS, accompanied by a 30–40 wt% of oxygen, similar to the carbon steel. When zoomed to

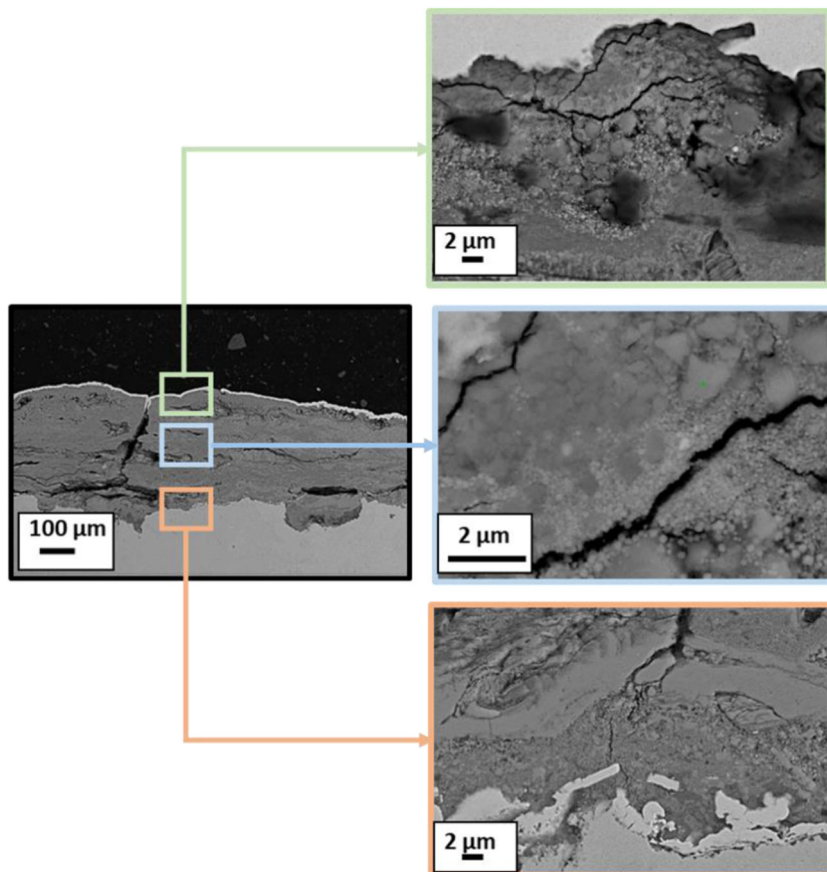


**FIGURE 8** SEM study of a cross-section of the carbon steel specimen exposed in vapor/condensate phase over a 1 mol/l HCl solution. SEM, scanning electron microscope. [Color figure can be viewed at [wileyonlinelibrary.com](http://wileyonlinelibrary.com)].

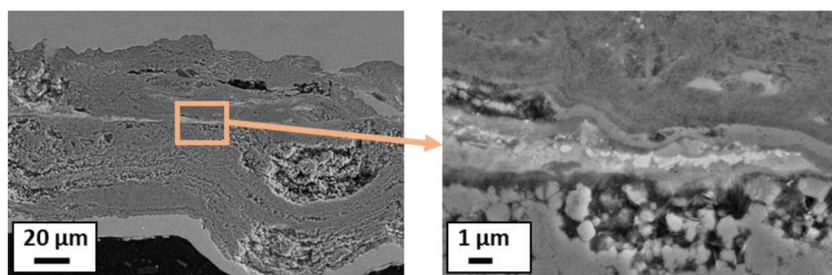


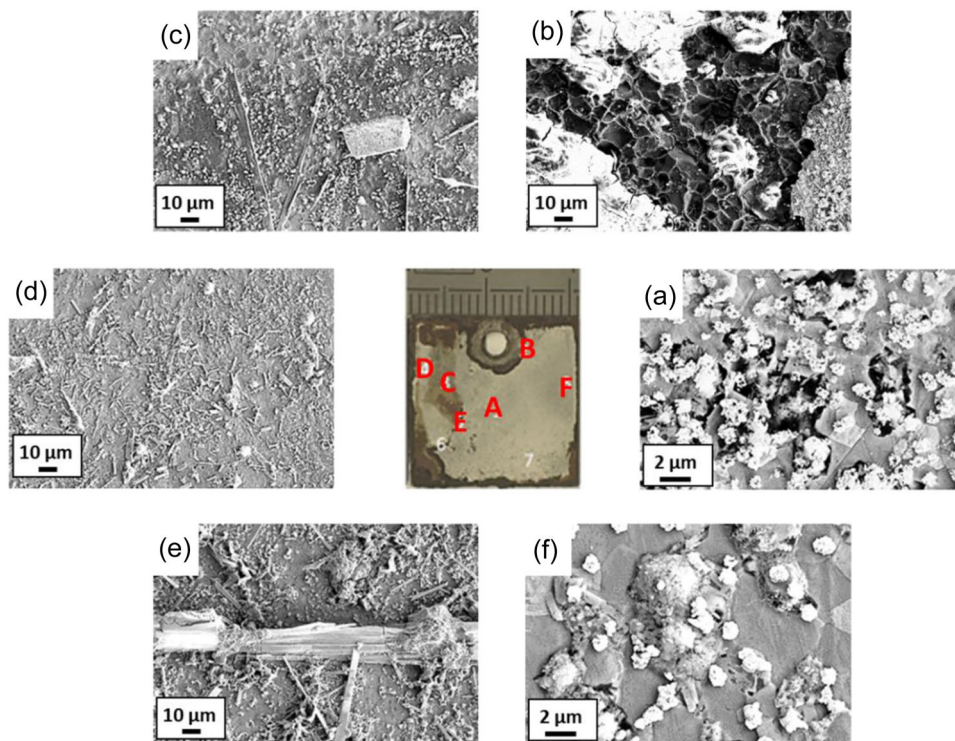
**FIGURE 9** SEM cross-section study of the tinned steel specimen exposed in vapor/condensate phase over a 1 mol/l HCl solution, with a zoom on the level of the thin white line. SEM, scanning electron microscope.

an  $\times 5000$  objective, the characteristic structure of lepidocrocite is visible with the oxide present in the sand rose form. No lead trace is detected. In the two cases, iron is corroded, and for the tinned steel, no more trace of the coating layer is visible except at the level of the Sn white strip.

As tests progress, the error bars become more important. These error bars are calculated on the mass measurement of three samples per test time. The different facies from one sample to another explain these error bars: corrosion is not homogeneous and depends on the condensates' position during the test. Moreover, the

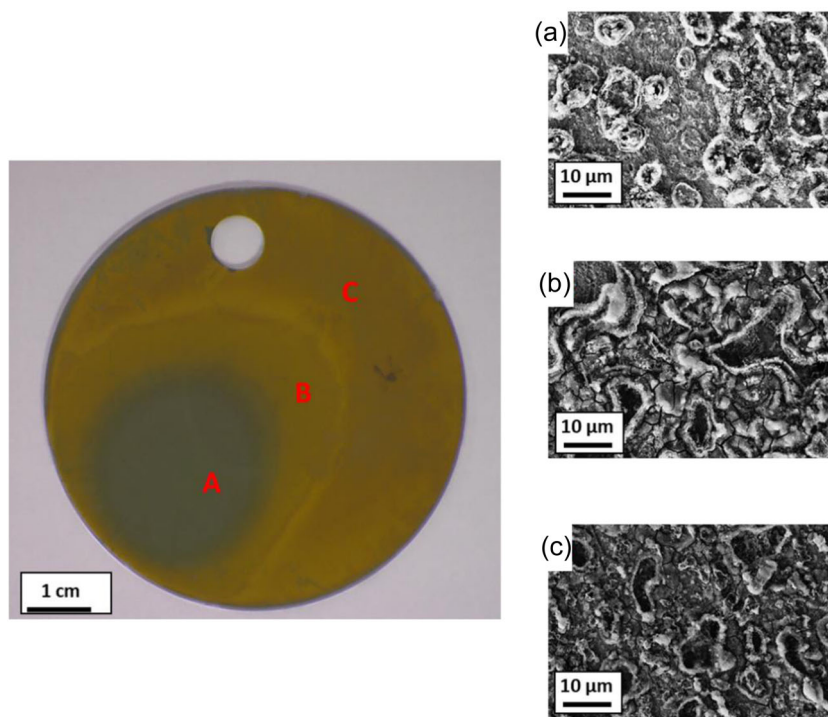
macrographs in Figure 7 show that the corrosion is not homogenous in intensity. The longer the exposure time, the more marked the corrosion.

Figure 10 shows the SEM analysis of the sample exposed 983 h over an HCl solution. In the center (zone A), the matrix is still visible accompanied by cerussite islands. Around the fixing hole but outside of the area impacted by the cut (zone B), a clear demarcation appears between the corroded area and the tinning layer. If the tinning layer appears identical to zone A, in the corroded area, only iron is present accompanied by an oxide of 60 wt% of iron. This



**FIGURE 10** SEM study of the tinned steel specimen exposed to a vapor/condensate phase over a 1 mol/l HCl solution during 983 h; (b), (c), (d), and (e)  $\times 500$ , (a) and (f)  $\times 5000$ . SEM, scanning electron microscope. [Color figure can be viewed at [wileyonlinelibrary.com](http://wileyonlinelibrary.com)].

**FIGURE 11** SEM study of the low carbon steel specimen after 7 days of exposure to a humid airflow at 33% RH polluted by HCl at 4.8 ppm. RH, relative humidity; SEM, scanning electron microscope. [Color figure can be viewed at [wileyonlinelibrary.com](http://wileyonlinelibrary.com)]



composition approaches 70 wt% of iron and 30 wt% of oxygen if the other elements are not taken into account, which can correspond to iron oxide type  $\text{Fe}_3\text{O}_4$ . The presence of condensates is well delimited and identified

by zones C, D, and E. In these areas, lead chloride is visible either in the form of nodules or in the form of longitudinal crystals. Cerussite on its surface can be present in the form of crystals of about  $1 \mu\text{m}$ . These  $\text{PbCl}_2$

crystals are locally accompanied by tin oxide  $\text{SnO}_2$ , identified locally by EDS. On the other hand, when the coating is only locally oxidized, the cerussite seems to be accompanied by tin monoxide type Sn (Figure 10f).

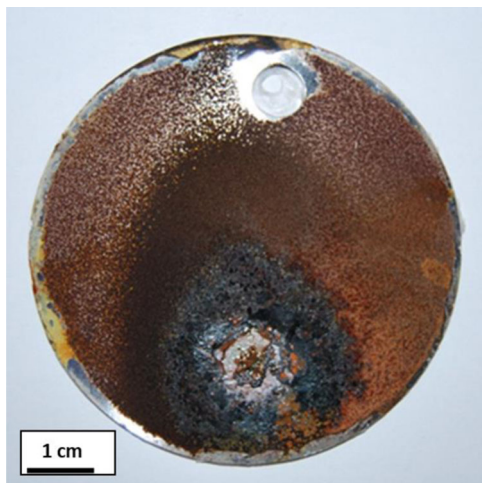


**FIGURE 12** SEM study of the low carbon steel specimen after 7 days of exposure to a humid airflow at 78% RH polluted by HCl at 4.8 ppm. RH, relative humidity; SEM, scanning electron microscope. [Color figure can be viewed at [wileyonlinelibrary.com](http://wileyonlinelibrary.com)].

### 3.4 | Dynamic tests in a humid air polluted by HCl

To be more realistic with a corrosion phenomenon that initiates on the material surface, samples were exposed to a humid air polluted by HCl flow.<sup>[27]</sup>

For the low carbon steel, after 7 days of testing, the sample is orange, indicating the presence of corrosion products (Figure 11). The corroded zone is delimited in three areas: the sample is darker in the area directly under the gas flow. A halo and a more weakly corroded side area surround this area. The corrosion layer is quite thin and nonvolatile. It is compact. Regardless of the location viewed, the corrosion facies is characterized by the presence of small cups on the surface. Note that even after 7 days of testing; the corrosion products are large enough to be mechanically stressed and to be cracked.

For a higher relative humidity, Figure 12 shows corrosion more marked with a color gradient from brown to black. Directly under the airflow polluted by HCl appears a gray area, it is the bare steel that shows a phenomenon of condensation located under the airflow that pushes the corrosion products. In this case, no SEM image was taken: the rinsing protocol does not include scraping the surface to remove the oxide layer, its use in

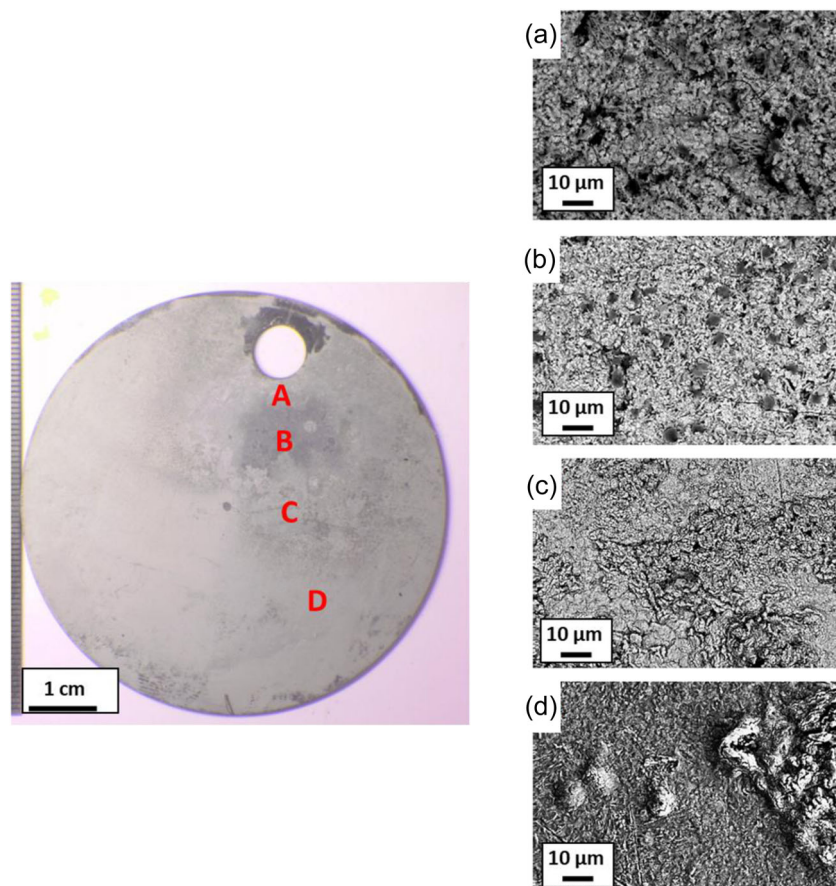


**FIGURE 13** SEM studies the tinned steel specimen after 7 days of exposure to a humid airflow at 33% RH polluted by HCl at 4.8 ppm. RH, relative humidity; SEM, scanning electron microscope. [Color figure can be viewed at [wileyonlinelibrary.com](http://wileyonlinelibrary.com)]

the SEM is very limited because the layered oxide is fragile and friable, which is polluting the SEM.

Figures 13 and 14 show the surface of the tinned sample exposed for 168 h to a flow of 33% and 76% relative humidity air polluted with hydrogen chloride.

Under the gas flow, a demarcation appears, materialized by different gray levels. The areas protected by a silicone seal as well as the edges of the sample and the gas discharge hole are intact, unlike the rest of the sample. This confirms that the whole surface of the sample is impacted by the gas flow.

Away from the flux and without protection,  $\text{PbCl}_2$  is present in the form of coarse grains (Figures 13a and 14a), their size increases as one approaches the zone impacted by the gas flow (Figure 14b), forming a compact but cracked layer (Figure 14c). The  $\text{PbCl}_2$  layer is raised, with prominent blisters (Figure 13d). This lead chloride layer is accompanied by a lamella rich in tin, chlorine, and oxygen, whose composition varies, which explains the different facies between SEM images (Figure 13b,c). The matrix is no longer visible.

For the test done in the highest relative humidity, the relief of the sample shows that a condensate must have formed at the level of the letter D in Figure 14. In this area, iron is the sole element detected with chlorine. Its content is

decreasing when we remove it from the zone under the gas flow until it is no longer detected (Figure 14a).

## 4 | DISCUSSION

A 75Sn–25Pb coating on low carbon steel and its support material have been studied in a humid and HCl-polluted environment to understand how this classical component of industry corrodes and to specify the different stages of the mechanism. In this sense, different experiments were conducted both on the Pb–Sn coating and on a bare low carbon steel, and also with and without HCl. The discussion is divided into three parts: one is dedicated to the corrosion behavior of the low carbon steel, the second one to the tinned steel corrosion and the third part gives answers to the title question: what happens when a Pb–Sn coating is deposited on low carbon steel is exposed in an HCl-polluted wet environment? Figures 15 and 16 summarize all the steps of the mechanism whose equations are presented in Table 3 and serve as a basis for the discussion.

Before testing, the coating consists mainly of tin, with the addition of lead plots. The layer is fine and covers a low carbon steel (Figures 15a and 16a).

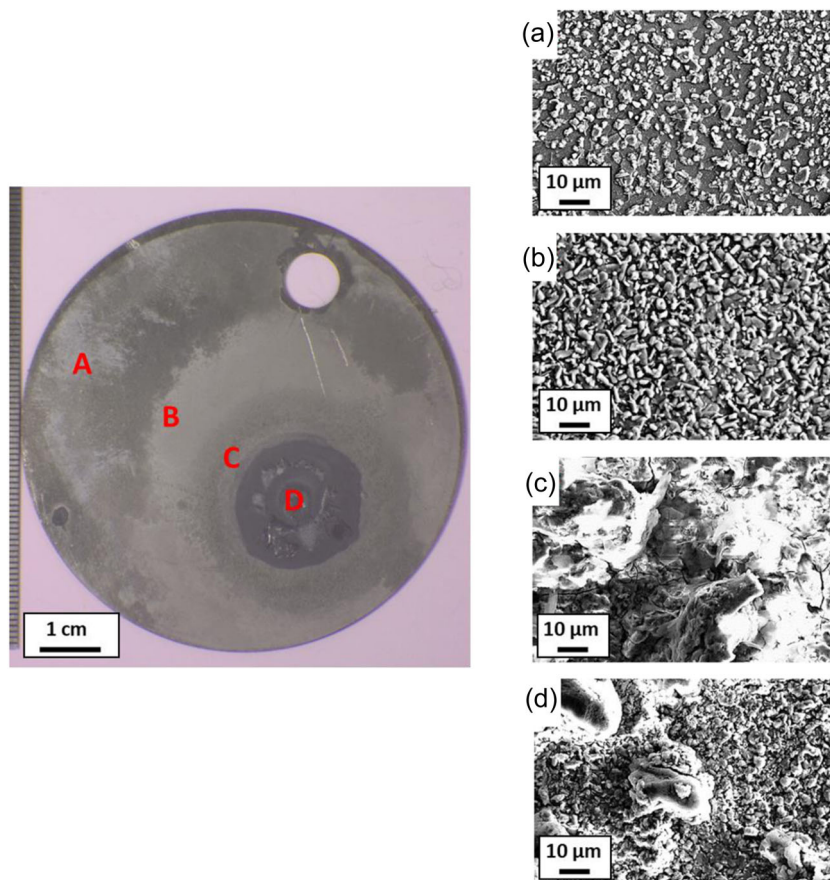


**FIGURE 14** SEM study of the tinned steel specimen after 7 days of exposure to a humid airflow at 76% RH polluted by HCl at 3 ppm, near the hole. RH, relative humidity; SEM, scanning electron microscope. [Color figure can be viewed at [wileyonlinelibrary.com](http://wileyonlinelibrary.com)].

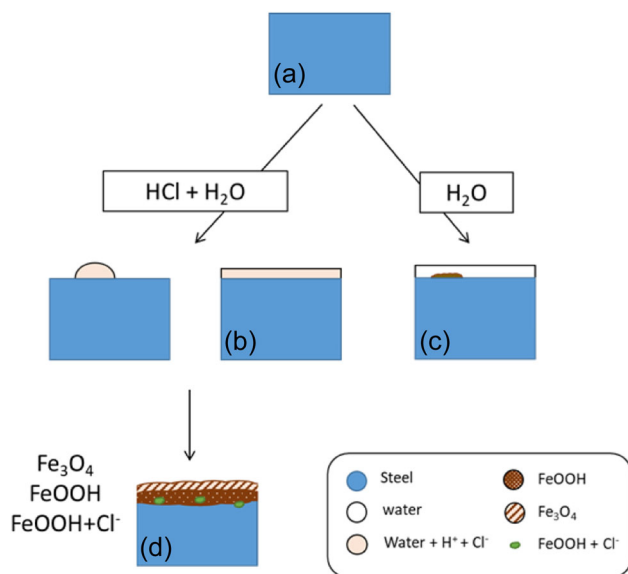


**FIGURE 15** Corrosion mechanism schemes of low carbon steel exposed to an HCl-polluted environment. Low carbon steel is blue and iron in brown. [Color figure can be viewed at [wileyonlinelibrary.com](http://wileyonlinelibrary.com)]

#### 4.1 | The low carbon steel corrosion mechanism

The element that corrodes in a low-carbon steel is iron. Exposed to a wet environment, iron corrodes (Figure 15c). The oxidation of iron is well known in the literature<sup>[30]</sup> and can be summarized as follows: initially, the oxygen in the air diffuses through the liquid film. It is reduced to OH<sup>-</sup> ions on the surface of the metal while the iron oxidizes to ferrous Fe<sup>2+</sup> ions, which go into solution in the electrolyte. The ferrous ions in the solution then react with dissolved oxygen to form different corrosion products like lepidocrocite ( $\gamma$ -FeOOH), goethite ( $\alpha$ -FeOOH), or akaganeite ( $\beta$ -FeOOH) (Equation 1).<sup>[31]</sup> The larger the FeOOH layer becomes and the more the reaction slows down because, on the one hand, the active iron surface decreases, and, on the other hand, the diffusion of oxygen is limited by the presence of the FeOOH layer. When the oxygen concentration becomes too low, lepidocrocite reacts with Fe<sup>2+</sup> ions in the aqueous phase to give the magnetite (Fe<sub>3</sub>O<sub>4</sub>) layer according to Equation (2).<sup>[32]</sup> The FeOOH rust, therefore, behaves as an oxidant with respect to iron in the same way as oxygen. The last reaction should stop when it has consumed all the rust, but in fact, the reduction of FeOOH only occurs in the aqueous phase with a low concentration of O<sub>2</sub>. If pollutants such as Cl<sup>-</sup> are present in the aqueous phase (Figure 15b), the consumption of the metal is accelerated<sup>[33]</sup> and local precipitation of corrosion products with trapped Cl<sup>-</sup> is obtained<sup>[34]</sup> (Figure 15d).

#### 4.2 | The Pb–Sn coating on a low carbon steel corrosion mechanism

Pourbaix studied the Pb–H<sub>2</sub>O and has established the domains of thermodynamic stability of lead and its compounds.<sup>[35]</sup> Lead can be seen to be a relatively noble metal from pH > 5, with the formation of PbO (Equation 3) but dissolving to Pb<sup>2+</sup> species at lower pH, as shown by the immersion test. Lead also passivates, with the formation of PbO<sub>2</sub> across the whole pH domain, but Pourbaix shows that it is for a higher potential value (Equation 4). In an acid medium, PbO is very soluble<sup>[36]</sup> in agreement with the dissolution observed in HCl solution. This leads to the formation of the Pb<sup>2+</sup> ions. PbO<sub>2</sub> is thermodynamically unstable in acid solution,<sup>[37]</sup> which explains why it has been little observed and contributed to creating ions. The electrolyte formed on the surface of samples is therefore charged with lead ions (Figure 16f). For tin, two oxides can be formed (Equations 6 and 7): SnO for the lower values of potential coupled with a pH between 3 and 9, and SnO<sub>2</sub> for higher values of potential but over a wider pH range.<sup>[37]</sup> The observations show that the surface can be coated with SnO. SnO<sub>2</sub> is present only in the form of a very thin, nondetectable surface layer with SEM.<sup>[38]</sup> For pH lower than two, tin forms the stannous ions Sn<sup>2+</sup>, which explains why the tin oxides were observed only occasionally.

Exposed to a vapor/condensate phase, the environment is made of HCl, steam, and air. A significant weight of CO<sub>2</sub> is present. When CO<sub>2</sub> is dissolved into water,<sup>[39]</sup> the reactions from Equation (8) to Equation (10) can take place, which lead to the formation of the carbonate ions CO<sub>3</sub><sup>2-</sup>. The carbonate ions are dissolved in the electrolyte and can form with lead cerussite PbCO<sub>3</sub> (Equation 11, (Figure 16g,n)). No tin carbonate is observed. The thermodynamic value of Equation (12) shows that this reaction is possible.<sup>[40]</sup> However, only one thermodynamic data is available. Even if thermodynamics inclined to say that the formation of carbonates is possible, the thermodynamic data comparison and the experiment results confirm that only oxides are formed. In areas where samples are particularly corroded, the cerussite is predominantly present but locally accompanied by SnO<sub>2</sub>. While at another level, tin is pure, accompanied by small crystals of PbCO<sub>3</sub>.

The association of HCl-steam leads to the creation of a finite size electrolyte, which is acid, and chlorinate charged. In contact with the electrolyte, cerussite evolves into lead chloride (Equation 14 and Figure 16h). This reaction is not direct. It involves intermediates compounds formation like paralaurionite PbCl(OH). However, their compositions vary. As an example, in geology,

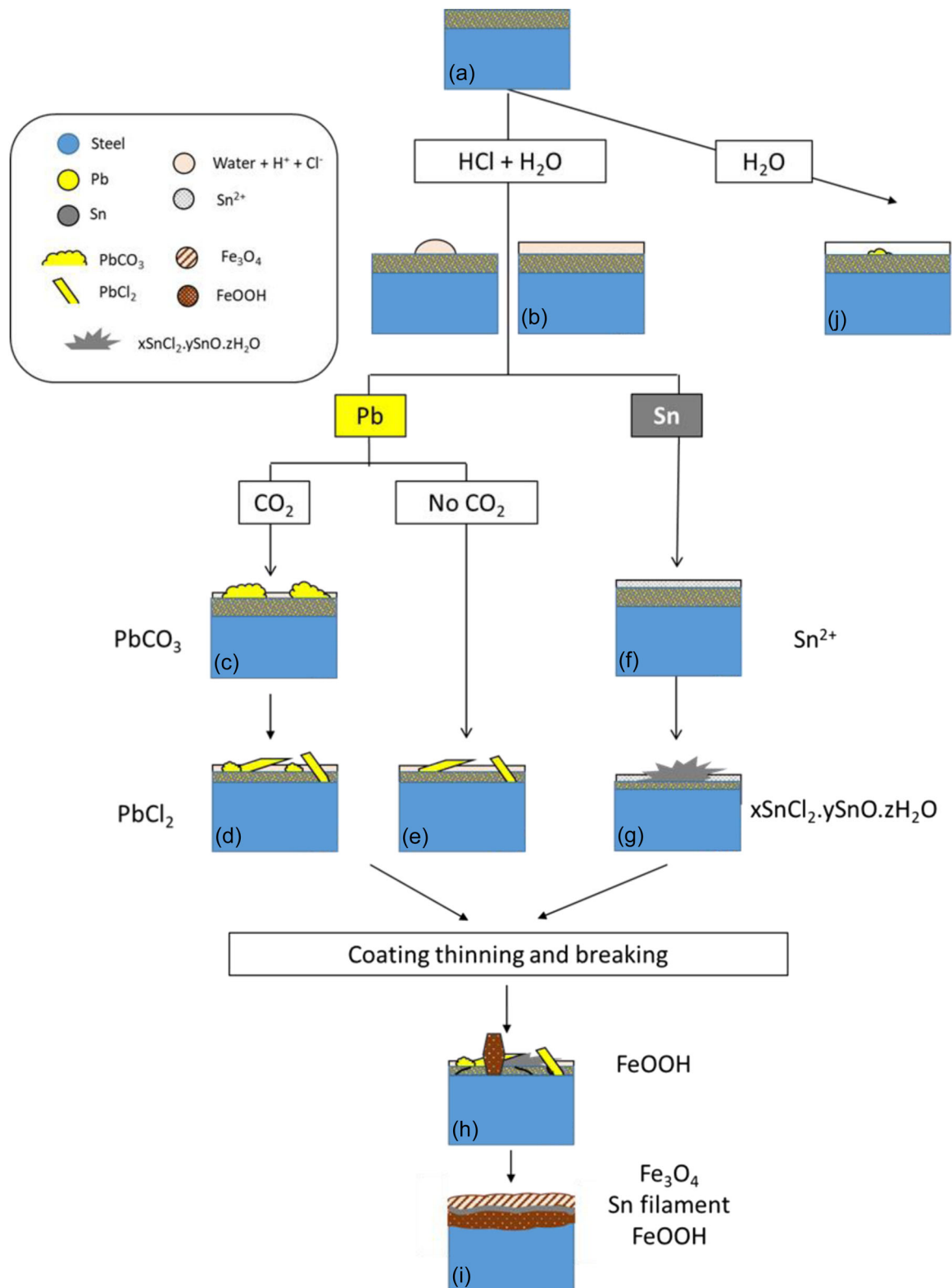


**FIGURE 16** Corrosion mechanism schemes of the 75Sn–25Pb coating layer on a low carbon steel exposed to an HCl-polluted environment. Low carbon steel is in blue, lead is in yellow, tin is in gray, and iron in brown. [Color figure can be viewed at [wileyonlinelibrary.com](http://wileyonlinelibrary.com)].

TABLE 3 Balance equation of the reactions involved in the corrosion mechanism of low carbon steel and exposed to a humid and polluted environment

Number	Equation	Log K
Equation (1)	$2\text{Fe}^{2+} + \frac{1}{2}\text{O}_2 + 3\text{H}_2\text{O} = 2\gamma - \text{FeOOH} + 4\text{H}^+$	log K = 83.73
Equation (2)	$8\gamma - \text{FeOOH} + \text{Fe} = 3\text{Fe}_3\text{O}_4 + 4\text{H}_2\text{O}$	log K = 177.74
Equation (3)	$\text{Pb}(\text{s}) + \frac{1}{2}\text{O}_2(\text{g}) = \text{PbO}(\text{s})$	log K = 33.97
Equation (4)	$\text{Pb}(\text{s}) + \text{O}_2(\text{g}) = \text{PbO}_2(\text{s})$	log K = 39.25
Equation (5)	$\text{PbO}(\text{s}) + 2\text{H}^+(\text{l}) = \text{Pb}^{2+}(\text{l}) + \text{H}_2\text{O}(\text{l})$	log K = 13.03
Equation (6)	$\text{Sn}(\text{s}) + \frac{1}{2}\text{O}_2(\text{g}) = \text{SnO}(\text{s})$	log K = 45.32
Equation (7)	$\text{Sn}(\text{s}) + \text{O}_2(\text{g}) = \text{SnO}_2(\text{s})$	log K = 92.76
Equation (8)	$\text{CO}_2(\text{g}) + \text{H}_2\text{O} = \text{H}_2\text{CO}_3(\text{l})$	log K = -1.46
Equation (9)	$\text{H}_2\text{CO}_3(\text{l}) = \text{H}^+ + \text{HCO}_3^-(\text{l})$	log K = -6.36
Equation (10)	$\text{HCO}_3^-(\text{l}) = \text{H}^+ + \text{CO}_3^{2-}(\text{l})$	log K = -10.33
Equation (11)	$\text{Pb}^{2+}(\text{l}) + \text{CO}_3^{2-}(\text{l}) = \text{PbCO}_3(\text{s})$	log K = 12.94
Equation (12)	$\text{Sn}^{2+}(\text{l}) + \text{CO}_3^{2-}(\text{l}) = \text{SnCO}_3(\text{s})$	log K = 10.95
Equation (13)	$\text{PbO}_2(\text{s}) + \text{SnO}(\text{s}) = \text{PbO}(\text{s}) + \text{SnO}_2(\text{s})$	log K = 42.16
Equation (14)	$\text{PbCO}_3(\text{s}) + 2\text{HCl}(\text{l}) \rightarrow \text{PbCl}_2 + \text{H}_2\text{O}(\text{l}) + \text{CO}_2(\text{g})$	log K = 23.37
Equation (15)	$\text{Pb}_3\text{O}_2\text{Cl}_2 + 2\text{CO}_2 + 2\text{H}_2\text{O}(\text{l}) \rightarrow \text{Pb}_3(\text{CO}_3)_2(\text{OH})_2 + \text{HCl}(\text{l})$	
Equation (16)	$\text{Pb}^{2+}(\text{l}) + 2\text{Cl}^-(\text{l}) = \text{PbCl}_2(\text{s})$	log K = 4.81
Equation (17)	$(x + y)\text{Sn} + (x/2 + y/2)\text{O}_2 + 2x\text{HCl} + (z - x)\text{H}_2\text{O} = x\text{SnCl}_2 \cdot y\text{SnO} \cdot z\text{H}_2\text{O}$	

it is shown that the formation of hydrocerussite  $\text{Pb}_3(\text{CO}_3)_2(\text{OH})_2$  first passes through the formation of mendite  $\text{Pb}_3\text{O}_2\text{Cl}_2$  with the formation of HCl (Equation 15). Nevertheless, no thermodynamic data exists on these different intermediate compounds due to their composition variability and probably their instability.

According to Equation (14), a part of the carbon dioxide is reformed. On the one hand, it can continue to maintain the reaction of Equation (11). On the other hand, it can react according to the reaction of Equation (15). This gas consumption explains why the cotunnite  $\text{PbCl}_2$  is observed from the first reactor opening during the intermediate test over the solution (Figure 16i): the  $\text{Pb}^{2+}$  ions do not have enough  $\text{CO}_3^{2-}$  dissolved to form cerussite and react directly with HCl forming  $\text{PbCl}_2$  (Equation 16). This result is in accordance with the dynamic flow test, where the tinned steel specimens are exposed to a very pure  $\text{CO}_2$ -free airflow polluted by HCl. The only lead-based corrosion product observed is  $\text{PbCl}_2$ , or  $\text{PbCl}_2 \cdot 2\text{H}_2\text{O}$  (Figure 16i).

As the corrosion products grow, they form a compact  $\text{PbCl}_2$  layer that is highly mechanically stressed. Indeed the difference in the density between  $\text{PbCl}_2$ :  $5.8 \text{ g cm}^{-3}$  and Pb:  $11.3 \text{ g cm}^{-3}$ , leads to the cracks' formation creating HCl diffusion pathways to steel.

In parallel and due to the acidity of the electrolyte, tin dissolves and the electrolyte concentrates in  $\text{Sn}^{2+}$  (Figure 16j). The difference between Sn and Pb in HCl appears from the fact that  $\text{SnCl}_2$  is soluble in  $\text{HCl}(\text{l})$ , contrary to  $\text{PbCl}_2$ .<sup>[41]</sup> This is in accordance with the latency period necessary to observe tin-based compounds: the electrolyte has to be saturated with  $\text{Sn}^{2+}$  ions before tin compounds precipitate (Figure 16j). As tin reacts with  $\text{HCl}(\text{l})$ , the coating layer becomes thinner. As soon as the electrolyte is saturated with the stannous ions, tin-based products in the form of slats accompany cotunnite  $\text{PbCl}_2$  (Figure 16k). Their composition is variable. If oxides such as abhurite  $\text{Sn}_{21}\text{Cl}_{16}(\text{OH})_{14}\text{O}_6$  or hydroromarchite  $\text{Sn}_6(\text{OH})_4\text{O}_4$  can be envisaged (although they have not been explicitly identified), Matzko et al.<sup>[42]</sup> show that it is difficult to predict the tin corrosion products because there are many forms of the  $x\text{SnCl}_2 \cdot y\text{SnO} \cdot z\text{H}_2\text{O}$  type, each with a different x, y, and z following the Equation (17). The phases formed depend on the surrounding medium and the acidity of the solution.

After a certain exposure time, the Pb consumption added to the lead-based products' fragility and to the thinning of the 75Sn–25Pb coating leads to exposing the base metal to the electrolyte. The steel is then in contact with  $\text{HCl}(\text{l})$  and oxidizes (Figure 16d,l), creating stable

compounds. These oxides are observed on the surface of both low carbon and tinned steel samples exposed over an HCl solution, with however the border of tin to differentiate the two (Figure 16m). It should be noted that the lead is no longer present, which shows the fragility of the corrosion products and the nonadhesion of the lead-based corrosion products during the test.

### 4.3 | What happens when a Pb–Sn coating deposited on low carbon steel is exposed in an HCl-polluted wet environment?

Gaseous chlorine at low temperature and in the absence of moisture is not particularly corrosive. However, if any water is present, chlorine becomes aggressive to many metals. That is why chlorides resulting from the formation of HCl are pollutants that can be lethal for electronic equipment<sup>[43]</sup> and why the correct selection of corrosion protection methods in an acidic environment is very vital.<sup>[44–47]</sup> Although many improvements have been made to avoid its presence, the lack of air renewal can still today lead to the local formation of humid and HCl polluted air.

When HCl pollutes humid air, condensation tends to be favored,<sup>[48]</sup> creating an acid chloride concentrated electrolyte. In contact with this electrolyte, a corrosion phenomenon can initiate forming ions of a + 2 valence. This result is in agreement with literature relating that in a humid environment with chlorides, metals like Cu, Ag, Sn, and Pb migrate upon dissolution and deposit at the cathode. This is the electrolytic migration and is a typical form of corrosion found on electronic systems.<sup>[49]</sup> The formation of these ions can lead to the precipitation of natural corrosion products such as oxides. Both tin and lead-rich Pb–Sn alloys form SnO during the initial exposure of oxide-free surfaces to oxygen. When metallic tin becomes totally depleted from the surface, lead is oxidized on the Pb–Sn surface to yield mixed oxide.<sup>[50]</sup> The fact of having the two elements Pb and Sn also tends to promote oxidation as shown by Equation (13): the presence of tin promotes the oxidation of lead and it is possible to form SnO<sub>2</sub> from SnO via the presence of lead.<sup>[6]</sup> As the PbO solubility is high in HCl, the interaction between the two elements improves consequently the formation of cerussite, a bulky and fragile corrosion product. That is why CO<sub>2</sub> is qualified as a contaminant in electronic<sup>[51]</sup> and attention is paid to the storage of the Pb–Sn alloy in sliding bearing.<sup>[46]</sup>

In fact, during the corrosion process, the formed products consume and thin the Pb–Sn layer. Since the layer is not uniform, the local consumption of one of the

constituents can lead to the local perforation of material, which can no longer play its role due to a lack of material. As they are covered with corrosion products, the absence of a component forming small holes is not always visible which explains why a visual analysis is not sufficient to explain the failures.<sup>[47]</sup>

In our tests, two materials were studied: the Pb–Sn alloy in the form of a coating on low carbon steel and the steel itself. The choice of the support material was not made at random but is linked to the potential galvanic coupling, which can appear between the lead-tin alloy and the iron or its oxides. Galvanic corrosion occurs when cathodic and anodic metals are in contact in humid, salty, or outside environments, and when the potential of the two metals is different. Lead-tin is less noble than stainless steel but more noble than most other elements in common use like low carbon steel.<sup>[52]</sup> If iron is in contact with a more corrosion-resistant metal such as tin, or lead, the other metal can act as a cathode that greatly increases the rate of reduction of oxygen. Because the reduction of oxygen is coupled to the oxidation of iron, this can result in an increase in the rate at which iron is oxidized at the anode. This completes the explanation of the formation of the rough surface in the dynamic test at high relative humidity and under the gas flow, where the condensation in the form of a droplet may explain the greater corrosion but does not explain the absence of lead or tin corrosion products. On the other hand, the fact of detecting iron and iron-based corrosion products shows that the exposure of the metal surface must be able to lead to a galvanic coupling between the coating and the base metal, which explains this strong local corrosion.

Nevertheless, if tin is usually ineffective as a sacrificial anode due to its very low self-corrosion rate and generally may be safely used in contact with most materials<sup>[53]</sup>; as coatings on a printed circuit board assembly (PCBA), tin and SnAgCu solder (SAC) are found to be active.<sup>[12]</sup> Moreover, in running water circuits, it is well known that contact between lead and iron or its oxides leads to the formation of lead ions that pollute the water.<sup>[54]</sup> This shows that a corrosive environment is characterized by its physical and chemical nature, which may affect the electrochemical properties.<sup>[52]</sup> This is why it is important to predict corrosion phenomena.

Generally, if the materials are not selected by considering corrosion behavior as an important criteria/parameter, for example in electronics,<sup>[12]</sup> nowadays the corrosion problem is becoming bigger and more important due to its cost and the Pb non-eco-friendly problem. In this sense, to avoid/minimize the corrosion phenomenon, solutions are put in place with for example a cement

mortar-lined ductile iron for minimizing the lead release to drinking water<sup>[54]</sup> or with a Pb content that is minimized when solder must be exposed to a chloride-contain solution<sup>[49,55]</sup> or by the addition of corrosion inhibitors.<sup>[56-58]</sup> Nevertheless, this is only possible by understanding the corrosion mechanism step by step, as presented in this article, to have adapted protection.

## 5 | CONCLUSION

A mechanism of corrosion has been established for a 75Sn-25Pb coating on low carbon steel exposed to an HCl-polluted environment, based on the different experiments that have been carried out both in the liquid and in the gaseous environment.

In HCl solution, the tinned coating dissolves as the low carbon steel, leading to loss of material.

In an HCl-polluted environment, coupled with water, acid chlorides from the HCl(g) provide an aggressive electrolyte particularly favorable to corrosion. In contact with this electrolyte, lead products are created as PbCO<sub>3</sub> and PbCl<sub>2</sub>. In parallel, the electrolyte concentrates in Sn<sup>2+</sup> until saturation and tin precipitates under different forms. Due to the lead consumption, the lead corrosion products layer breaks and the coating thinning, diffusion pathways are created and the steel oxidizes. Iron corrosion products are similar with or without a coating except for the presence of a tin-rich filament. Lead is no longer present. This shows the special precautions that must be taken in the event of corrosion due to nonadherent and poorly protective lead corrosion products.

The different stages of the mechanism are compared to corrosion phenomena observed during the use of Pb-Sn alloys. They show the importance of knowing each step of the corrosion process to provide effective solutions to minimize or even avoid the phenomenon of corrosion.

## ACKNOWLEDGEMENTS

Open Access Funding provided by COUPERIN hybrid - Commissariat a l'energie atomique et aux energies alternatives Siege administratif.

## DATA AVAILABILITY STATEMENT

Data available on request from the authors.

## ORCID

Florence Lequien  <http://orcid.org/0000-0001-8022-3615>

## REFERENCES

- [1] H. Ipser, H. Flandorfer, C. Luef, C. Schmetterer, U. Saeed, in *Lead-Free Electronic Solders: A Special Issue of the Journal of Materials Science: Materials in Electronics*, Springer US, Boston, MA **2007**, p. 3.
- [2] J. W. Osenbach, J. M. DeLuca, B. D. Potteiger, A. Amin, F. A. Baiocchi, in *Lead-Free Electronic Solders: A Special Issue of the Journal of Materials Science: Materials in Electronics*. Boston, MA: Springer US **2007**, 283. pp. 283-305.
- [3] K. Subramanian, *Lead-Free Electronic Solders: A Special Issue of the Journal of Materials Science: Materials in Electronics*, Springer US, Boston, MA **2007**.
- [4] S.-R. Lim, J. M. Schoenung, *J. Hazard. Mater.* **2010**, *177*, 251.
- [5] L. Meng, J. Gao, Y. Zhong, Z. Wang, K. Chen, Z. Guo, *Sep. Purif. Technol.* **2018**, *191*, 375.
- [6] S. P. Tembhare, B. A. Bhanvase, D. P. Barai, S. J. Dhoble, *Environ. Dev. Sustain.* **2021**, 1-83.
- [7] L. Nazari, C. C. Xu, M. B. Ray, *Advanced and Emerging Technologies for Resource Recovery from Wastes*, Springer, New York **2021**, p. 127.
- [8] T. Dilmi, A. Guelil, A. Dakhouch, *Algerian J. Chem. Eng.* **2021**, *1*(1), 1-7.
- [9] J. Xu, X. Liu, X. Li, E. Barbero, C. Dong, *J. Power Sources* **2006**, *155*(2), 420.
- [10] S. Kaur, A. Kaur, P. S. Singh, T. Singh, *Prog. Nucl. Energy* **2016**, *93*, 277.
- [11] M. Uemura, *Science* **2002**, *14*(3), 321.
- [12] Jellesen MS, Verdingovas V, Conseil H, Piotrowska K, Ambat R, Eds. *European Corrosion Congress 2014*.
- [13] R. Hienonen, R. Lahtinen, *Corrosion and Climatic Effects in Electronics*, VTT Technical Research Centre of Finland, Espoo **2007**.
- [14] G. Zichittella, J. Pérez-Ramírez, *Angew. Chem.* **2021**, *133*, 24291.
- [15] Panayotova M, Panayotov V, Eds. *E3S Web of Conferences*, EDP Sciences **2021**.
- [16] A. Dal Pozzo, G. Muratori, G. Antonioni, V. Cozzani, *Waste Manage.* **2021**, *125*, 303.
- [17] Q. Lu, X. Zhou, Y. Wu, T. Mi, J. Liu, B. Hu, L. Zhao, *Chem. Eng. J.* **2021**, *425*, 130604.
- [18] Y.-H. Kiang, *Chem. Eng.* **1981**, *88*(3), 127.
- [19] M. N. Mohamed, N. Aziz, A. A. Mohamad, M. F. M. Nazeri, *Int. J. Electroactive Mater.* **2015**, *3*, 28.
- [20] E. Gouda, I. Faquhi, S. Kariri, M. Qohal, Y. Kariri, *Int. J. Mater. Sci. Appl.* **2015**, *4*(1), 8.
- [21] V. Brusica, D. D. DiMilia, R. MacInnes, *Corrosion* **1991**, *47*(7), 509.
- [22] I. D. Ryck, E. V. Biezen, K. Leysens, A. Adriaens, P. Storme, F. Adams, *J. Cult. Herit.* **2004**, *5*(2), 189.
- [23] G. Kreysa, M. Schütze, *Corrosion Handbook: Corrosive Agents and Their Interaction With Materials. Sodium Hydroxide, Mixed Acids*, John Wiley & Sons Inc, New York **2004**.
- [24] J. Vimala, M. Natesan, S. Rajendran, *Open Corros. J.* **2009**, *2*, 105.
- [25] L. Yougkui, *J. Univ. Sci. Technol. Beijing* **1989**, *11*(2), 167.
- [26] R. A. Konetzki, Y. A. Chang, V. C. Marcotte, *J. Mater. Res.* **2011**, *4*(6), 1421.
- [27] F. Lequien, G. Moine *Mater. Corros.* **2018**, *69*(10), 1422.
- [28] F. Lequien, G. Moine, A. Lequien, D. Neff, *Mater. Corros.* **2021**, *72*(9), 1488.

- [29] D. Vantelon, A. Lanzirotti, A. C. Scheinost, R. Kretzschmar, *Environ. Sci. Technol.* **2005**, 39(13), 4808.
- [30] M. HÉLIE, *Ellipses*, **2015**.
- [31] R. M. Cornell, U. Schwertmann, *The Iron Oxides: Structure, Properties, Reactions, Occurrences and Uses*, John Wiley & Sons, New York **2003**.
- [32] J. Chivot, Fonctions thermodynamiques, diagrammes de solubilité, diagrammes E-pH des systèmes Fe-H<sub>2</sub>O, Fe-CO<sub>2</sub>-H<sub>2</sub>O, Fe-S-H<sub>2</sub>O, Cr-H<sub>2</sub>O et Ni-H<sub>2</sub>O en fonction de la température. Thermodynamique des produits de corrosion. Châtenay-Malabry ANDRA, France.
- [33] G. Palanisamy, Corrosion Inhibitors, Intechopen, London **2019**.
- [34] S. Réguer, P. Dillmann, F. Mirambet, *Corros. Sci.* **2007**, 49(6), 2726.
- [35] M. Pourbaix, *Atlas of Electrochemical Equilibria in Aqueous Solutions*, National Association of Corrosion Engineers, Houston, TX **1974**.
- [36] M. Pourbaix, *Atlas d'équilibres électrochimiques*, Gauthier-Villars, Paris **1963**.
- [37] L. Leitch, Design, product development and risk assessment of tin (Sn) ring electrodes as a substitute to silver-silver chloride (AG AgCl) ring electrodes for high definition transcranial direct current stimulation (HD-tDCS). **2013**.
- [38] E.E.d Kluzenaar, *J. Vac. Sci. Technol. A* **1983**, 1(3), 1480.
- [39] S. K. Lower, Simon Fraser University. **1999**, 544. <http://www.chem1.com/acad/pdf/c3carb.pdf>. (accessed: 1999).
- [40] B. Lothenbach, M. Ochs, H. Wanner, M. Yui, *Thermodynamic Data for the Speciation and Solubility of Pd, Pb, Sn, Sb, Nb and Bi in Aqueous Solution*, Japan Nuclear Cycle Development Inst. **1999**.
- [41] B. White, *Anti-Corros. Methods Mater.* **1989**, 36(11), 7.
- [42] J. J. Matzko, H. T. Evans, M. E. Mrose, *Canad. Mineral.* **1985**, 23(2), 233.
- [43] P. Viswanadham, S. Canumalla, in *Corrosion: Environments and Industries* (Eds: S. D. Cramer, B. S. Jr. Covino), 13C: ASM International, Materials Park **2006**.
- [44] O. O. Ogunleye, A. O. Arinkoola, O. A. Eletta, O. O. Agbede, Y. A. Osho, A. F. Morakinyo, J. O. Hamed, *Heliyon* **2020**, 6(1), e03205.
- [45] N. A. Reza, N. H. Akhmal, N. A. Fadil, M. F. M. Taib, *Metals* **2021**, 11(7), 1062.
- [46] Z. Hu, X. Jie, G. Lu, *J. Coat. Technol. Res.* **2010**, 7(6), 809.
- [47] P. T. Vianco **1999**, *Corrosion Issues in Solder Joint Design and Service*, Sandia National Labs., Albuquerque, NM.
- [48] Y. Kiang, *Chem. Eng.* **1981**, 88(3), 127.
- [49] X. Zhong, L. Chen, B. Medgyes, Z. Zhang, S. Gao, L. Jakab, *RSC Adv.* **2017**, 7(45), 28186.
- [50] J. S. Vimala, M. Natesan, S. Rajendran, *Open Corros. J.* **2009**, 2, 105.
- [51] E. M. Bumiller, D. A. Douthit, J. Pecht, *Contamination of Electronic Assemblies*, CRC Press, **2002**.
- [52] X. Zhang, *Uhlig's Corrosion Handbook*, Vol. 51, WILEY & Sons, New York **2011**, p. 123.
- [53] T. Hoar, *Trans. Faraday Soc.* **1934**, 30, 472.
- [54] B. F. Trueman, G. A. Sweet, M. D. Harding, H. Estabrook, D. P. Bishop, G. A. Gagnon, *Environ. Sci. Technol.* **2017**, 51(12), 6812.
- [55] S.-B. Lee, H.-Y. Lee, M.-S. Jung, Y.-B. Park, Y.-C. Joo, *Met. Mater. Int.* **2011**, 17(4), 617.
- [56] H. Bentrach, A. Chala, Université Mohamad Khider, BISKRA **2015**.
- [57] N. Helal, M. El-Rabiee, G. M. Abd El-Hafez, W. Badawy, *J. Alloys Compd.* **2008**, 456(1-2), 372.
- [58] B. Krawczyk, P. Cook, J. Hobbs, D. L. Engelberg, *Corrosion* **2017**, 73(11), 1346.

**How to cite this article:** F. Lequien, G. Moine, A. Lequien, D. Neff, *Mater. Corros.* **2022**, 1–15.  
<https://doi.org/10.1002/maco.202213142>